Available online at www.sciencedirect.com
SCIENCE DIRECT®
Journal of Solid State Chemistry 178 (2005) 792–799
JOURNAL OF SOLID STATE CHEMISTRY
www.elsevier.com/locate/jssc

A new layered cobaltite $(Ga_{1/3}Co_{2/3})_2Sr_2CoO_{6+\delta}$ with high spin Co^{3+}: modulated structure and physical properties

D. Pelloquin*, S. Hébert, O. Perez, V. Pralong, N. Nguyen, A. Maignan

Laboratoire CRISMAT, UMR CNRS-EnsiCaen 6508, 6 bd Maréchal Juin, 14050 Caen Cedex, France

Received 18 October 2004; received in revised form 10 December 2004; accepted 10 December 2004

Abstract

Investigations in the Sr–Co–Ga–O system by means of transmission electron microscopy techniques have allowed the detection of a new layered cobaltite. Its structure has been obtained by combining high-resolution images and powder X-ray diffraction. The modulated structure of this novel oxide, $(Ga_{1/3}Co_{2/3})_2Sr_2CoO_{6+\delta}$ is derived from the perovskite with $a = a_p\sqrt{2}$, $b = a_p\sqrt{2}$, $c = 19.2\,\text{Å}$ and a modulation vector $q^* = q_1a^* + q_2c^*$. For the as-prepared samples, the δ value is close to 0.4 and the modulated structure ($q_1 \approx 1/3$ and $q_2 = 1$) can be described in an ideal orthorhombic 3D supercell *Bb2b* with the unit cell parameters $a = 3a_p\sqrt{2} = 16.3030(5)\,\text{Å}$, $b = 5.4725(2)\,\text{Å}$ and $c = 19.2034(4)\,\text{Å}$. The layer stacking consists in an intergrowth between a $[SrCoO_3]$ perovskite-type block and a block of triple layers, $[(SrO)(Co_{2/3}Ga_{1/3}O_{1+\delta/2})(Co_{2/3}Ga_{1/3}O_{1+\delta/2})]$ derived from [AO] rock-salt type layers. The magnetic study shows that the Co^{3+} cations exhibit a high spin state in this structure. The θ_p value, $-570\,\text{K}$, suggests that antiferromagnetic interactions dominate in this compound as in the brownmillerite cobaltites. Nonetheless, its resistivity $\rho_{300\,K} = 10^{-1}\,\Omega\,\text{cm}$ is lower than that of the brownmillerite compounds. Since the positive Seebeck coefficient indicates the presence of holes (Co^{4+}) in the CoO_2 conducting layers, the existence of weak ferromagnetic Co^{3+}–O–Co^{4+} interactions developing below $\approx 150\,\text{K}$ is proposed to explain the electronic properties of this new oxide.

Keywords: Cobalt oxide; Modulated layered structure derived from the perovskite; Transmission electron microscopy; Thermoelectric properties

1. Introduction

The search for new layered cobalt-based oxides is very important for discovering interesting physical properties, as recently illustrated by the discovery of a large thermoelectric power in the metallic phase Na_xCoO_2 ($x = 0.5$) [1], in the misfit related cobaltites [2–4], and by the report on the superconductivity ($T_c = 4.5\,\text{K}$) of the derived hydrated compound $Na_{0.3}CoO_2 \cdot 1.3H_2O$ [5]. More recently, the possibility to intercalate water molecules in the $Sr_{n+1}(Co,Ti)_nO_{3n+1}$ magnetic oxides related to the Ruddlesden Popper series has also been shown [6]. These results emphasize the richness of cobalt-based layer systems for which the cobalt mixed valency and spin-states play crucial role in the electronic and magnetic properties. As previously shown in the $Ln_{1-x}Ae_xCoO_3$ perovskite structures (for instance Ae = Sr and Ln = La), magnetoresistance properties related to the coexistence of Co^{4+} and Co^{3+} species are observed [7,8]. Furthermore, the physical properties of the perovskite compounds are sensitive to the cobalt coordination. This is the case of $LnBaCo_2O_{5.5}$ '112'-type cobaltites for which ordering of the Ln/Ba cations and of oxygen vacancies generates planes of CoO_6 octahedra alternating with planes of $[CoO_5]_2$ tetragonal bipyramids. Although they contain only Co^{3+}, this polyhedra ordering is responsible for both metal to insulator transition and magnetoresistance [9–11]. Among the layered cobaltites derived from the perovskite, the brownmillerite structure is also a candidate in generating new properties. In the structure of the $Sr_2Co_2O_5$

*Corresponding author. Fax: +33 2 31 96 16 00.
E-mail address: denis.pelloquin@ensicaen.fr (D. Pelloquin).

0022-4596/$ - see front matter © 2005 Elsevier Inc. All rights reserved.
doi:10.1016/j.jssc.2004.12.035

brownmillerite [12,13], the oxygen vacancies order to form alternating layers of CoO_6 corner-shared octahedra and chains of CoO_4 tetrahedra. A similar kind of structure has also been reported for $Sr_2Co_{2-x}Ga_xO_5$ ($0.3 \leqslant x \leqslant 0.8$) in which the tetrahedra are mixed sites occupied by either cobalt or gallium [14]. However, the ability for both cobalt and gallium species to adopt other coordinations such as octahedral or trigonal bipyramidal for gallium [15] and octahedral or square pyramidal or trigonal bipyramidal for cobalt [16] suggests that a more complex layer structure than the brownmillerite could be stabilized.

In the present paper, we report on the synthesis of a new layer oxide, $(Ga_{1/3}Co_{2/3})_2Sr_2CoO_{6+\delta}$, for which the modulated structure, derived from the perovskite, exhibits close relationships to the $Sr_4Fe_6O_{13-\varepsilon}$ ferrite [17–19] and $Bi_2Sr_2CoO_{6+\delta}$ 2201-type cobaltites [20,21]. Magnetic and electronic properties of polycrystalline samples of this new phase are also reported and discussed.

2. Experimental

In order to avoid the formation of the $Sr_2Co_{2-x}Ga_xO_5$ brownmillerite, oxidizing conditions obtained by using the decomposition of the SrO_2 peroxide in sealed tubes have been used. Two sets of samples have been prepared from stoichiometric mixtures of SrO/SrO_2, Ga_2O_3 and Co_3O_4 precursors: the first with the $Sr_2Co_{2-x}Ga_xO_{5+\delta}$ composition and the second, after the first structural characterizations, with the $(Ga_{1/3}Co_{2/3})_2Sr_2CoO_{6+\delta}$ composition. The oxygen content has been controlled by changing the SrO/SrO_2 ratio. The mixtures were ground in an agate mortar, pressed in the form of bars and then placed in alumina finger. Then the samples were placed in quartz tube, the latter being sealed under primary vacuum before heating up to 1100 °C at a rate of 100 °C h^{-1}. After 12 h at 1100 °C, the tubes were then quenched in air and black ceramic bars were finally obtained. Powder X-ray diffraction data of the as-prepared bars were collected at room temperature using an XpertPro Philips vertical diffractometer working with the Cu$K\alpha$ radiation and equipped with a secondary graphite monochromator. Data collection was carried out by continuous scanning (step = $0.01°(2\theta)$, preset = 30 s) over an angular range $4° \leqslant 2\theta \leqslant 120°$. Lattice constants and structural calculations were refined by the Rietveld method using the software FULLPROF included in the WINPLOTR package [22]. Some of these as-prepared samples were also analyzed by means of transmission electron microscopy (TEM). The electron diffraction analysis has been carried out using a JEOL 200CX microscope fitted with an eucentric goniometer ($\pm 60°$) while the high resolution images have been recorded from a TOPCON 002B microscope (Cs = 0.40 mm). Both microscopes are equipped with a KEVEX analyzer (Energy Dispersive Spectroscopy).

The magnetic properties were studied using a SQUID magnetometer (ac and dc; 0–5 T; 1.8–400 K) and a Faraday balance (0.3T; RT-800 K). Resistance data as a function of temperature (1.8–400 K) or magnetic field (0–7 T) were collected with a quantum design physical properties measurement system (PPMS) by the four-probe technique. Current and voltage indium contacts were ultrasonically deposited on the sintered bars (typically $2 \times 2 \times 10$ mm). A steady-state method was used to measure the Seebeck effect (S) in the PPMS with high temperature limit fixed at 320 K by the calibration range of the temperature sensors.

Iodometric titrations were performed to determine the cobalt oxidation state of the as-prepared phases. The end-point is electrochemically determined by following the potential of the solution with platinum electrodes versus ECS electrode, while the current is held at zero. Each sample (ca. 50 mg) is dissolved in a molar acetic buffer solution (ca. 50 mL) containing an excess of KI (ca.1 g). Co^{3+} and Co^{4+} species are reduced to Co^{2+} together with formation of iodine species in a stoichiometric amount. Iodine is therefore titrated with $Na_2S_2O_3$ 0.1 N solution using thiodene (starch) as colorimetric indicator in addition to the potential evolution.

3. Results

The first obtained $Sr_2Co_{2-x}Ga_xO_{5+\delta}$ polycrystalline samples were found to be multiphasic from electron diffraction data and only few crystals with a brownmillerite-type structure were observed. Besides the identified different phases, $Sr_6Co_5O_{15}$ and $SrGa_2O_4$, numerous crystals exhibiting relationships with the perovskite structure with a stacking parameter close to 19 Å were detected. Note that this periodicity has not been observed in the Ga-free sample ($x = 0$). By considering TEM analytical results in the EDS mode, leading the nominal Ga content to the average cationic composition, "$Ga_{2/3}Sr_2Co_{7/3}$", new syntheses were prepared using the same thermal cycle but with different nominal oxygen stoichiometries. New samples have thus been synthesized starting from the $Ga_{2/3}Sr_2Co_{7/3}O_{6+\delta}$ compositions. It must be emphasized that for the samples prepared from oxygen contents below 6.5, the brownmillerite formation is favored showing that oxidizing conditions are necessary to stabilize this new cobaltite.

4. Structural analysis

The first analyses by TEM of the nominal $Ga_{2/3}Sr_2Co_{7/3}O_{6.5+\delta}$ sample, prepared by using SrO_2 only,

reveal a complex cell related to an intergrowth mechanism built from a perovskite-type subcell. The study of electron diffraction (ED) patterns allows us to identify a F-type orthorhombic subcell with $a \approx b \approx 5.4\,\text{Å}$ and $c \approx 19.2\,\text{Å}$ (Fig. 1), while the EDS analyses lead to the same average cationic composition "$Ga_{0.7}Sr_2Co_{2.3}$", i.e. a value close to the nominal compositions. In addition to these fundamental reflexions, extra spots are systematically observed along a^* and c^* axes as illustrated by the [010] and [001] ED patterns shown in Fig. 1 (white arrows). Depending on the studied zones of the crystals, these extra spots are in commensurate and/or incommensurate positions and sometimes are diffuse. In a conventional 3D reciprocal space, the corresponding supercell is especially difficult to deduce since a bidimensional modulation vector $q^* = q_1a^* + q_2c^*$ is necessary to explain these extra spots. For this compound, one obtains thus the component $q_2 = 1$ while the analysis of the image contrasts from the [001] oriented shows from the edge to the crystal core the existence of ordered contrasts with a various periodicity ($q_1 \approx 0.33,\ 0.43\ldots$). This suggests the coexistence of several nanostructural features. The complex positions of the detected extra spots could result from the superimposition of these different nanostructural features. Nonetheless, the tripling of the a parameter related to a component $q_1^* = 0.33a^*$, is often observed in the crystal edge in agreement with the intensity of extra spots observed in the ($h/6a^*$, 0) positions ($h = 2n$) of the [001] oriented ED patterns. Consequently, an ideal commensurate supercell, $3a_p\sqrt{2} \times a_p\sqrt{2} \times 19.2\,\text{Å}^3$, can be used to describe the structure of this new compound. Considering this orthorhombic lattice, the systematic reflection conditions $h\,k\,l$ ($h + l = 2n$), $0\,k\,l$ ($k + l = 2n$) and $h\,k\,0$ ($h + k = 2n$) are deduced. They are compatible with the *Bb*2*b* and *Bbmb* space groups.

In order to determine the number and the nature of the different layers stacked along the c direction, an HREM study has been carried out. This work has been performed on [$\bar{1}$30] and [010] oriented crystals. The [$\bar{1}$30] oriented image shown in Fig. 2, corresponding to the $[100]_p$ orientation in a perovskite structure, is the best

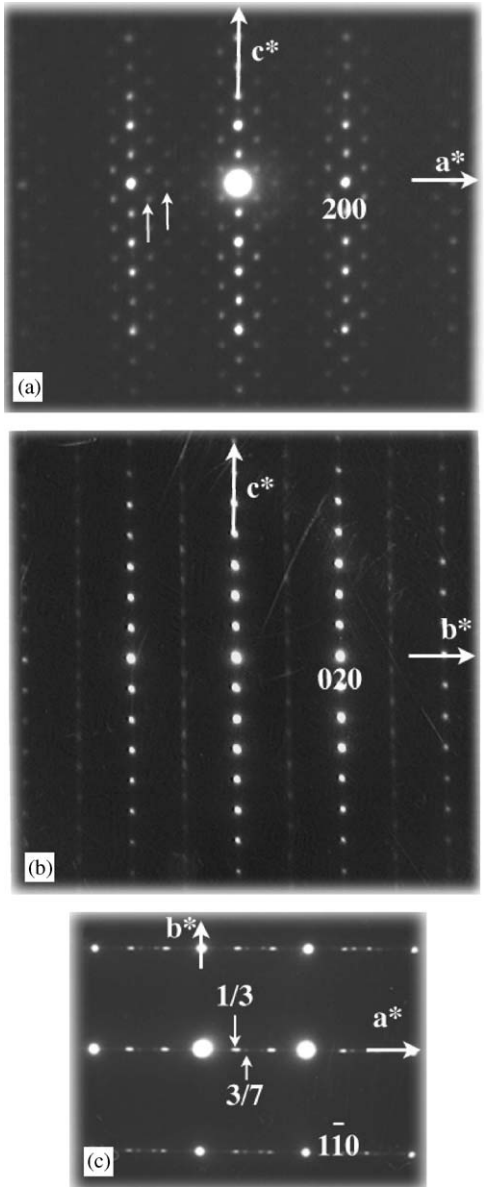

Fig. 1. Experimental electron diffraction patterns oriented along (a)-[010], (b)-[100] and (c)- [001] directions. The patterns are indexed in the subcell ($a = a_p\sqrt{2}$, $b = a_p\sqrt{2}$, $c = 19.2\,\text{Å}$) and the extra spots are pointed out by small white arrows.

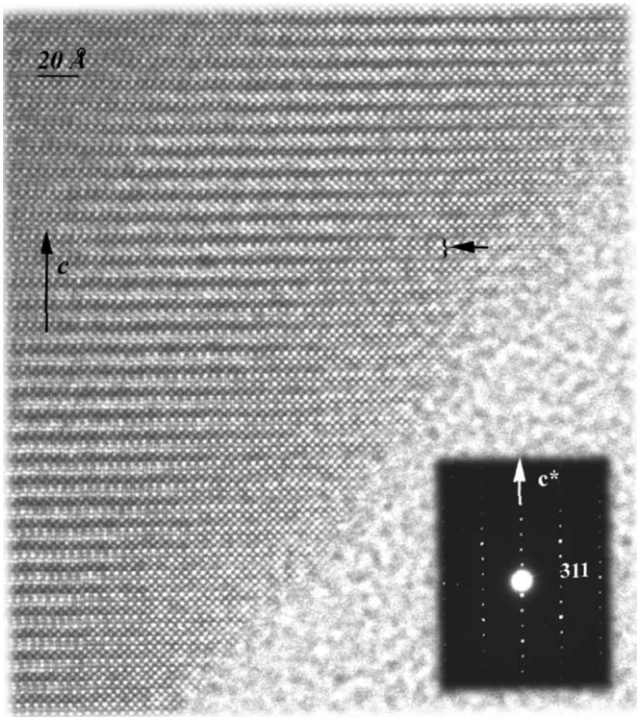

Fig. 2. Experimental [$\bar{1}$30] oriented ED pattern and corresponding HREM image. The perovskite-type slice is pointed out by a black arrow and bracket.

viewing direction to confirm the relationship with the perovskite structure and visualize the stacking mode along the *c*-axis. This image has been recorded with a defocus value $\Delta f \approx -450$ Å in which the high electron density zones are imaged as bright dots. At the edge of the crystal (black arrow in Fig. 2), blocks of three bright layers, about 3.9 Å thick and spaced about 5.7 Å along the *c*-axis by double rows of staggered similar gray dots, are observed. Clearly, the stacking mode corresponds to the regular intergrowth of five layers. The image contrasts and the spacing of rows in the first block (3.85 Å in-plane and 2.00 Å out of plane) are undoubtedly characteristic of a perovskite-type slice. The structure of the second block, formed of four rows of which the outer ones are common to both blocks, is more difficult to identify. In this respect, the analysis of the [010] oriented crystals is helpful and, moreover it also explains the origin of the supercell. The HREM [010] oriented images shown in Fig. 3 have been recorded with two different defocus values (Δf). The first one recorded with a $\Delta f \approx -250$ Å (Fig. 3a), for which the cation rows are correlated to the dark dots, shows at the edge of the crystal four rows of aligned bright dots, 2.70 Å spaced along **a**. These blocks, about 5.7 Å thick, are spaced along **c** by a row of gray dots. Such a contrast can be correlated to four [AO] rock-salt type layers intergrown with a $[MO_2]$ perovskite-type layer where *M* is a metal (*M* = Ga or Co). Interestingly, a periodic contrast variation running along **a**, as diffuse bright sticks (white arrow in Fig. 3a) alternating with gray sticks, is observed at the level of these four [AO] layers implying a possible ordering phenomena between the Ga and Co species. Taking into account the cationic composition deduced from EDS analyses, namely "$Ga_{0.7}Sr_2Co_{2.3}$", a regular intergrowth between a perovskite-type block, $SrCoO_3$, and three theoritical [AO] rock-salt type layers can be proposed according the following sequence:

$$(Ga_{1/3}Co_{2/3}O)-(Ga_{1/3}Co_{2/3}O)-SrO-CoO_2-SrO-(Ga_{1/3}Co_{2/3}O)-(Ga_{1/3}Co_{2/3}O)\ldots$$

Such a stacking mode leads to the ideal oxygen stoichiometry $(Ga_{1/3}Co_{2/3})_2Sr_2CoO_6$ formula.

The second image shown in Fig. 3b, recorded with a Δf value close to -500 Å, where the high electron density zones are correlated to the bright dots, is more representative. Clearly, four [AO] undulate with a periodicity of 6×2.70 Å along **a** to form periodic lips in phase and out of phase along the **c**-axis, in the same way as in the bismuth-based $Bi_2Sr_2CoO_{6+\delta}$ "2201"-type cobaltites [20,21]. A contrast as three aligned bright dots along **c**-axis is observed at the level of the nodal zone. In the thicker zone, the latter becomes a light checkerboard contrast (white circle in Fig. 3b) whereas the $[CoO_2]$ perovskite-type layer, disturbed according to the same periodicity, is displayed as a row of lighter dots. We assume that such a modulated structure results from the coexistence of different coordination polyhedra inside the double $(Ga_{2/3}Co_{4/3}O_2)$ layers. From this hypothesis and taking into account the main modulation component, implying the tripling of cells along the *a*-axis, a cationic framework can be proposed (Fig. 4).

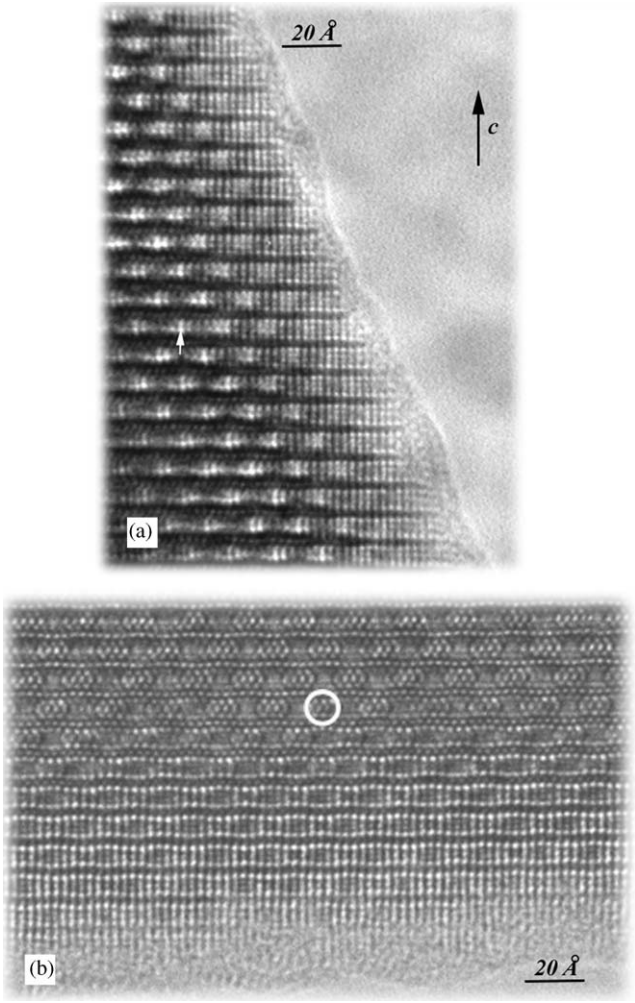

Fig. 3. Experimental [010] HREM images recorded with a defocus value close to (a) −250 Å and (b) −500 Å.

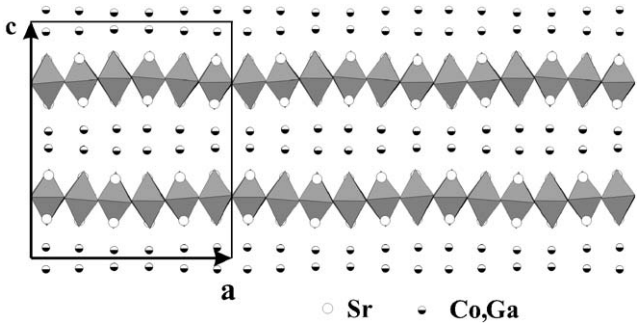

Fig. 4. Cationic framework of $(Ga_{1/3}Co_{2/3})_2Sr_2CoO_{6+\delta}$ deduced from TEM observations. The octahedra are for the CoO_6 planes.

Since gallium and cobalt species can adopt various coordination polyhedra such as octahedron or trigonal bipyramid or tetrahedron for Ga, and octahedron or square pyramid or trigonal bipyramid or tetrahedron for Co, the actual oxygen content inside these double layers could be greater than two. This hypothesis is confirmed by iodometric titrations performed on different as-prepared samples. They are systematically revealed to have an average formal state of +2.9 for cobalt species. Thus, an oxygen content around 6.4 can be deduced considering the "$(Ga_{2/3}Co_{4/3})Sr_2Co$" cationic composition. Consequently the double layers must be rewritten $(Ga_{2/3}Co_{4/3}O_{2+\delta})$, with an actual value $\delta \approx 0.4$ for the as-prepared compound. Thus, a correlation can be made between this oxygen excess and the modulated behavior of this new oxide.

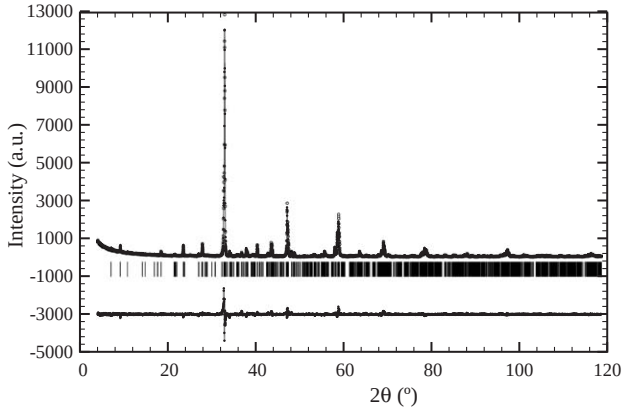

Fig. 5. Experimental, calculated and difference powder X-ray diffraction patterns of $(Ga_{1/3}Co_{2/3})_2Sr_2CoO_{6+\delta}$ This pattern is indexed in the orthorhombic 3D supercell *Bb2b* ($a = 16.3030(5)$ Å, $b = 5.4725(2)$ Å and $c = 19.2034(4)$ Å).

5. Average structure and oxygen non-stoichiometry

In order to validate the stacking mode and assume a first comparative structural analysis, refinements have been attempted from powder X-ray diffraction data. This work has been made considering an ideal *Bb2b* supercell, $3a_p\sqrt{2} \times a_p\sqrt{2} \times 19.2\,\text{Å}^3$, and starting with atomic positions deduced from HREM observations. With this superlattice, the refined unit cell parameters, $a = 16.3030(5)$ Å, $b = 5.4725(2)$ Å and $c = 19.2034(4)$ Å, fit well the overall powder X-ray pattern as shown in Fig. 5. In a first step, a model with stoichiometric double $(Ga_{2/3}Co_{4/3}O_2)$ rock-salt type layers has been considered without refining their oxygen positions. This model (Table 1) implies three independent cationic positions at the level of these double layers but any preferential occupation site between cobalt and gallium species could be detected in agreement with their closing scattering factors. The corresponding refinements lead to a poor reliability factor, $R_{bragg} \approx 0.20$. Next, these oxygen sites have been released and a Fourier difference analysis has been attempted at the level of these double $(Ga_{2/3}Co_{4/3}O_{2+\delta})$ layers in order to locate the $\delta \approx 0.4$ oxygen position in excess. The oxygen sites surrounding the Ga and Co species are shifted noticeably from their ideal position. In the same way, the displacements along

Table 1
Refined atomic positions of $(Ga_{1/3}Co_{2/3})_2Sr_2CoO_6$ in an ideal 3D model

Atoms	*x*	*y*	*z*	*B*(Å^2)	*n*
Ga/Co	0.0846 (12)	0.27125 (38)	0.0308 (10)	0.496 (51)	8
Ga/Co	0.2526 (10)	0.79315 (45)	0.0439 (67)	0.496 (51)	8
Ga/Co	0.4224 (19)	0.31208 (26)	0.0402 (70)	0.496 (51)	8
O1	0.5000 (0)	0.00000 (0)	0.0471 (35)	1.0*	4
O2	0.2287 (37)	0.50000 (0)	0.0505 (28)	1.0*	8
O3	0.1570 (38)	0.00000 (0)	0.0362 (25)	1.0*	8
O4	0.3382 (41)	0.50000 (0)	0.0000 (0)	1.0*	4
Sr1	0.0862 (7)	0.75000 (0)	0.1526 (4)	0.970 (21)	8
Sr2	0.2528 (7)	0.25000 (0)	0.1602 (5)	1.064 (28)	8
Sr3	0.4123 (6)	0.75000 (0)	0.1644 (4)	0.424 (20)	8
O5	0.0668 (30)	0.25000 (0)	0.1176 (22)	1.0*	8
O6	0.3008 (28)	0.75000 (0)	0.1294 (24)	1.0*	8
O7	0.4259 (39)	0.25000 (0)	0.1344 (18)	1.0*	8
Co1	0.0806 (10)	0.25000 (0)	0.2429 (64)	0.663 (61)	8
Co2	0.2500 (0)	0.75000 (0)	0.25000 (0)	1.079 (82)	4
O8	0.0050 (35)	0.50000 (0)	0.2500 (24)	1.0*	8
O9	0.3337 (44)	0.00000 (0)	0.2826 (21)	1.0*	8
O10	0.1702 (38)	0.50000 (0)	0.2433 (24)	1.0*	8
$a = 16.3031(5)$ Å					
$b = 5.4725(1)$ Å		SG:*Bb2b*		Bragg *R*-factor = 0.141	
$c = 19.2034(4)$ Å					

*not refined.

the **c**-axis of Ga and Co positions sitting in these peculiar layers are consistent with the specific undulation, like periodic lips, of these double layers observed in the HREM images. At the end of these refinements, a significant decrease of the reliability factor to $R_B \approx 0.14$, is obtained. This result validates the structural framework shown in Fig. 4 even though no significant extra oxygen position at the level of $(Ga_{2/3}Co_{4/3}O_{2+\delta})$ layers could be deduced from this powder X-ray diffraction data set. If one takes into account the numerous nanostructural features observed by TEM observations, this result is not unexpected.

Nonetheless, at this stage of the analysis, a structural relationship can be made with the $Sr_4Fe_6O_{13-\varepsilon}$ [17–19] and the 2201-type $Bi_2Sr_2CoO_{6.25}$ [20] oxides, which exhibit also a similar undulated stacking mode but with a different modulation component along **a**, $q_1^* \approx 0.40a^*$ and $0.24a^*$, respectively. In the $Sr_4Fe_6O_{13-\varepsilon}$ oxides, two types of iron polyhedra, namely square pyramids and trigonal bipyramids, have been reported at the level of double iron-based layers. It has been demonstrated that their distribution is intimately correlated to the amount of extra oxygens inserted in the $[Fe_2O_{2+\varepsilon}]$ layers, illustrated by the $q_1 = (1-\varepsilon)/2$ relation [18,19]. In the case of the modulated Bi-based 2201-type oxide, the equivalent double layers are mainly composed of Bi^{3+} species surrounded by three or four oxygens which leads to BiO_3L tetrahedra and BiO_4L trigonal bipyramids, where L is the lone pair of Bi^{3+} [21]. Consequently, the coexistence of several kinds of polyhedra, tetrahedra, square pyramids and trigonal bipyramids in the aforementioned double layers can be discussed. Since the Ga species can adopt the trigonal bipyramidal coordination, we can assume that the Co species adopt preferentially the square pyramidal and/or tetrahedral coordinations. The impossibility of isolating the Ga-free compound, $Sr_2Co_3O_{6+\delta}$, strongly supports this point of view. However a structural analysis from single crystal X-ray diffraction data based on a superspace formalism, to take into account the irrational components of the q vector, will be necessary to solve the structure and describe more exactly this complex distribution. This work will require a single crystal of this new phase to be grown.

The origin of the different modulation vectors observed in the ED study can be associated to several nanostructural features. First, the Co/Ga ratio can locally change implying a new arrangement between the CoO_x and GaO_x polyhedras. Secondly, the nature of the polyhedra, in these peculiar layers, is probably more dependent on the oxygen content like previously demonstrated for $Sr_4Fe_6O_{13-\varepsilon}$ [18,19] The last point is illustrated by a post-synthesis treatment undertaken at 400 °C under Ar/H_2 flow (90:10) on the as-prepared $(Ga_{1/3}Co_{2/3})_2Sr_2CoO_{6+\delta}$ sample ($\delta = 0.4$). The iodometric titrations reveal an average formal state of +2.6 for the cobalt species leading to $\delta \approx 0$. This result is confirmed by the E.D study undertaken after this annealing. Clearly, the modulation is affected by this post-synthesis treatment since a modulation vector such as $q^* \approx 0.30a^* + c^*$ vector is observed, compared to the initial $q^* = 0.33a^* + c^*$ value.

6. Magnetic and electronic properties

One particularity of the magnetic properties of the cobaltites crystallizing in the brownmillerite structure is the strong antiferromagnetism characterized by a high T_N value ($T_N = 570$ K for $Sr_2Co_2O_5$ [12]). This feature results from the strong 180° Co^{3+}–O–Co^{3+} superexchange between neighboring high-spin Co^{3+} ($S = 2$). It must be emphasized that the Co^{3+} high-spin configuration, rather unique to brownmillerite, results from the large dilatation of the CoO_6 octahedra in this structure [13,14,23]. By taking into account the stoichiometry of the new oxide under study, $(Ga_{1/3}Co_{2/3})_2Sr_2CoO_{6.40}$, it turns out that the average cobalt oxidation state is mainly trivalent. This is confirmed by magnetic measurements: an effective moment $\mu_{eff} = 4.85\mu_B$/Co is extracted by Curie–Weiss fitting in the T range 300–800 K of the reciprocal magnetic susceptibility data measured in 0.3 T (Fig. 6). This is very close to the theoretical value for high-spin Co^{3+} ($4.9\mu_B$). Clearly, the spin-state configuration of the cobalt cations is also high spin in this new $(Ga_{1/3}Co_{2/3})_2Sr_2CoO_{6.40}$ cobaltite, suggesting that the CoO_6 octahedra in the perovskite-type slice are elongated in this structure. The lack of a clear antiferromagnetic transition on the $\chi^{-1}(T)$ curve up to 800 K suggests that

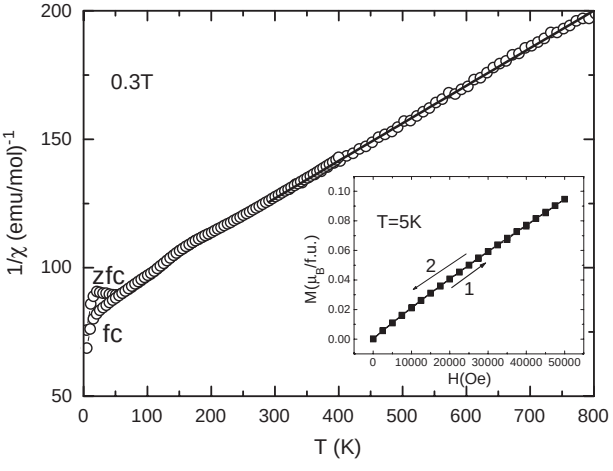

Fig. 6. Inverse of susceptibility $\chi^{-1}(T)$ under 0.3 T in zero field and field cooled mode between 5 and 400 K. The straight line corresponds to the Curie–Weiss fitting (see text). Inset: $M(H)$ half-loop recorded at 5 K. The arrows "1" and "2" are for the increasing and decreasing magnetic field, respectively.

this transition is smeared. This is probably due to the larger spacing between two successive perovskite CoO_2 layers than in the brownmillerite [14] which decreases the interlayer magnetic coupling. Most probably, the exchange in the CoO_2 plane is stronger than from plane to plane through the mixed (Co/Ga)O layers. This situation is similar to other layer cobaltites such as $Bi_2Sr_2CoO_{6+\delta}$ [24]. At $T = 5\,K$, isothermal magnetic field (H) dependent magnetization (M) measurements (inset of Fig. 6) are also in agreement with antiferromagnetism. The $M(H)$ curves are linear in the 0–5 T field range with very low M values in 5 T, leading to only small magnetic moments per cobalt, e.g. $M_{5\,K}^{5\,T} = 0.1\mu_B$/Co. Such a low value could be easily explained by considering the field-induced small canting between the antiparallel magnetic moments. The resistivity measurements performed by cooling the sample from 400 K down to 5 K in the absence and in the presence of a 7 T magnetic field (Fig. 7) show that this sample exhibits a low resistivity in the high T region, for instance $\rho = 0.1\,\Omega\,cm$ at 300 K. In principle, this value is not consistent with the presence of only pure high-spin Co^{3+} cations ($\rho_{300\,K} \sim 10^2 - 10^3\,\Omega\,cm$ for the $Sr_2Co_2O_5$ [13] brownmillerite). According to the presence of different crystallographic sites in the separating layers between successive perovskite layers, one cannot exclude that part of the cobalt exhibits a different oxidation state and/or spin state. To check the nature of the charge carriers, thermoelectric power measurements have been performed. The T dependence of the Seebeck coefficient (S), given in Fig. 8, shows $S > 0$ for all temperatures in the range $5\,K \leqslant T \leqslant 320\,K$ which indicates that "holes" govern the transport properties of this oxide. Possibly, a slight amount of Co^{4+} in the majority Co^{3+} matrix could account for the hole character of the charge carriers. By comparing the $S_{300\,K}$ value, $+30\mu V\,K^{-1}$, to

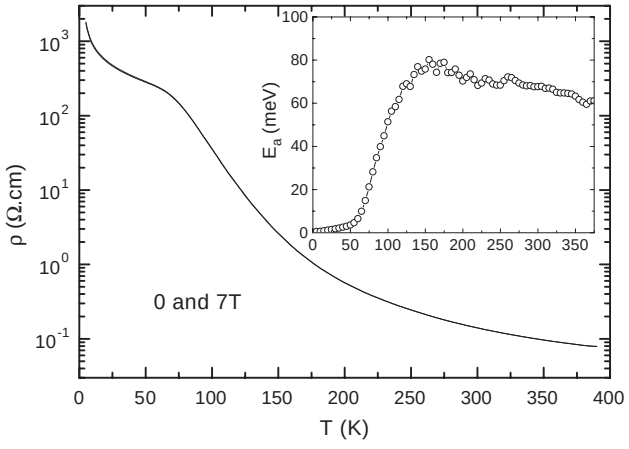

Fig. 7. $\rho(T)$ curves measured under 0 and 7 T upon cooling from 390 K. In the whole T range, the two curves are superimposed. Inset: local activation energy as a function of T. Below about $\approx 125\,K$, a clear decrease is observed.

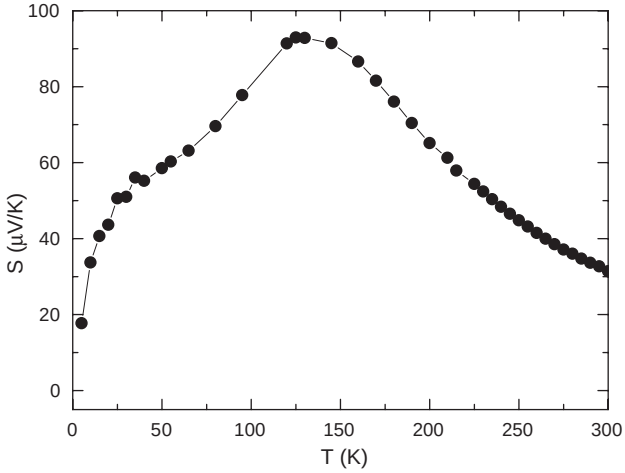

Fig. 8. Seebeck coefficient S as a function of T.

those reported for the series $La_{1-x}Sr_xCoO_3$ [25], a similar S value is obtained for $x = 0.15$, i.e. for 15% Co^{4+} per cobalt. Such a hole concentration could be obtained in $(Ga_{1/3}Co_{2/3})_2Sr_2CoO_{6+\delta}$ by considering a rather large oxygen overstoichiometry, $O_{6.675}$ instead of $O_{6.4}$, or the existence of Co^{2+} in the modulated layers separating the perovskite layers, which would create a corresponding charge transfer in the plane of CoO_6 octahedra.

Finally, the origin of the slope change at about 50 K on the $\rho(T)$ curve, associated to a divergence between the fc and zfc curves (Fig. 6) at about the same temperature, is unknown. It could come from the presence of a magnetic impurity ($Sr_6Co_5O_{15}$) or from the existence of short-range and weak Co^{3+}–O–Co^{4+} ferromagnetic interaction in the antiferromagnetic matrix.

This point is consistent with the S maximum close to $+95\mu V\,K^{-1}$ on the $S(T)$ curve at $T \approx 150\,K$. The S decrease below that temperature indicates a change of conduction regime toward a less semi-conducting regime compatible with the Co^{3+}/Co^{4+} local ferromagnetic interactions. This is corroborated by the small change of slope observed on the $\chi^{-1}(T)$ curve at $T \approx 150\,K$ (Fig. 6) suggesting also the appearance of ferromagnetic interactions. This decrease of the activation energy can be observed from the T dependence of the local activation energy given in the inset of Fig. 7. For T greater than $\approx 150\,K$, the activation energy is of about 60–80 meV, whereas this energy decreases below $\approx 125\,K$, indicating that the transport mechanism starts to change. Below about 60 K, this activation energy, smaller than 10 meV, supports that small ferromagnetic metallic regions develop without reaching the percolation threshold. Note also that no significant magnetoresistance is found from the comparison of the $\rho_{0\,T}$ and $\rho_{7\,T}$ curves. At that point of the study, a more detailed structural model must be refined to establish more

definitive conclusions about the origin of the properties of this new cobalt oxide.

7. Conclusions

A new layer Ga-based cobaltite, $(Ga_{1/3}Co_{2/3})_2Sr_2CoO_{6+\delta}$, has been isolated. This oxide can be described as a regular intergrowth between a $[SrCoO_3]$ perovskite-type block and a block of triple layers, $[(SrO)(Co_{2/3}Ga_{1/3}O_{1+\delta/2})(Co_{2/3}Ga_{1/3}O_{1+\delta/2})]$ derived from [AO] rock-salt type layers. Interestingly its complex structural features exhibit close relationships with the modulated bismuth-based 2201-type structures $Bi_2Sr_2CoO_{6+\delta}$ and the ferrite $Sr_4Fe_6O_{13-\varepsilon}$. Like the latter, oxygen non-stoichiometry has been detected with a δ value ranging from 0 (post-synthesis annealing) to about 0.40 (as-prepared). However, a fine structural analysis from single crystal X-ray diffraction and neutron powder diffraction data based on a superspace formalism is required to analyze the different metal environments and their distribution inside the double $(Ga_{2/3}Co_{4/3}O_{2+\delta})$ layers. This work coupled with a comparative study between calculated and experimental HREM images is necessary to describe more exactly this complex lattice and its evolution depending on the oxygen non-stoichiometry value. Moreover it will allow the establishment of more definitive conclusions about the origin of the properties of this new cobaltite resulting from the high-spin state of the cobalt cations. The control of the cobalt valence state by an oxidizing/reducing electrochemical process and the study of the oxygen-sorptive and -desorptive properties are in progress.

References

[1] I. Terasaki, Y. Sasago, K. Uchinokura, Phys. Rev. B 56 (1997) 12685.
[2] A.C. Masset, C. Michel, A. Maignan, M. Hervieu, O. Toulemonde, F. Studer, B. Raveau, J. Hejtmanek, Phys. Rev. B 62 (2000) 166.
[3] A. Maignan, S. Hébert, D. Pelloquin, C. Michel, J. Hejtmanek, J. Appl. Phys. 92 (2002) 1964.
[4] A. Maignan, S. Hébert, M. Hervieu, C. Michel, D. Pelloquin, D. Khomskii, J. Phys.: Condens. Matter 15 (2003) 2711.
[5] K. Takada, H. Sakurai, E. Takyama-Mutomachi, F. Izumi, R.A. Dilanian, T. Sasaki, Nature 422 (2003) 53.
[6] D. Pelloquin, N. Barrier, D. Flahaut, V. Caignaert, A. Maignan, Chem. Mater. (2005) in press; D. Pelloquin, N. Barrier, D. Flahaut, V. Caignaert, A. Maignan, Solid State Sci. (2005) in press.
[7] S. Yamaguchi, H. Taniguchi, H. Takagi, T. Arima, Y. Tokura, J. Phys. Soc. Jpn. 64 (1995) 1885.
[8] S. Yamaguchi, Y. Okimoto, H. Taniguchi, Y. Tokura, Phys. Rev. B 53 (1996) R2926.
[9] C. Martin, A. Maignan, D. Pelloquin, N. Nguyen, B. Raveau, Appl. Phys. Lett. 71 (1997) 1421.
[10] A. Maignan, C. Martin, D. Pelloquin, N. Nguyen, B. Raveau, J. Solid State Chem. 142 (1999) 247.
[11] C. Frontera, J.L. García-Munoz, A. Llobet, M.A.G. Aranda, Phys. Rev. B 65 (2002) R180405.
[12] T. Takeda, Y. Yamaguchi, H. Watanabe, J. Phys. Soc. Jpn. 33 (1972) 970.
[13] J.C. Grenier, S. Ghodbane, G. Demazeau, M. Pouchard, P. Hagenmuller, Mat. Res. Bull. 14 (1979) 831.
[14] F. Lindberg, S. Ya. Istomin, P. Berastegui, G. Svensson, S.M. Kazakov, E.V. Antipov, J. Solid State Chem. 173 (2003) 395.
[15] A.M. Abakumov, M.G. Rozova, A.M. Alekseeva, M.L. Kovba, E.V. Antipov, O.I. Lebedev, G. Van Tendeloo, Solid State Sci. 5 (2003) 871.
[16] S.Ya. Istomin, J. Grins, G. Svensson, G.A. Drozhzhin, V.L. Kozhevnikof, E.V. Antipov, J.P. Attfield, Chem. Mater. 15 (2003) 4012.
[17] F. Kanamaru, M. Shimada, M. Koizumi, J. Phys. Chem. Solids 33 (1972) 1169.
[18] M.D. Rossel, A.M. Abakumov, G. Van Tendeloo, J.A. Pardo, J. Santiso, Chem. Mater. 13 (2004) 2578.
[19] B. Mellenne, R . Retoux,, C. Lepoitevin, M. Hervieu, B. Raveau, Chem. Mater. 16 (2004) 5006.
[20] J.M. Tarascon, P.F. Miceli, P. Barboux, D.M. Hwang, G.W. Hull, M. Giroud, L.H. Greene, Y. Lepage, W.R. McKinnon, E. Tselepis, G. Pleizier, M. Eibschutz, D.A. Neumann, J.J. Phyne, Phys. Rev. B 39 (1989) 11587.
[21] N. Jakubowicz, D. Grebille, H. Leligny, M. Evain, J. Phys. Condens. Matter 11 (1999) 3997.
[22] J. Rodriguez-Carvajal, Fullprof, in:, J. Galy (Ed.), Collected abstracts of powder diffraction meeting, Toulouse, France, p. 127.
[23] Y. Takeda, R. Kauno, T. Takada, O. Yamamoto, M. Takano, Y. Bando, Z. Anorg. Allg. Chem. 540/541 (1986) 259.
[24] K.J. Thomas, Y.S. Lee, F.C. Chou, B. Khaykovich, P.A. Lee, M.A. Kastner, R.J. Cava, J.W. Lynn, Phys. Rev. B 66 (2002) 054415.
[25] M.A. Senaris-Rodriguez, J.B. Goodenough, J. Solid State Chem. 118 (1995) 323.